Topography and Force Imaging in Atomic Force Microscopy by State and Parameter Estimation*

Michael R. P. Ragazzon, J. Tommy Gravdahl, Kristin Y. Pettersen, and Arnfinn A. Eielsen

***Abstract*— A novel imaging method for atomic force microscopy based on estimation of state and parameters is presented. The cantilever dynamics is modeled as a linear system augmented by the tip-sample interaction force. The states of this augmented system are observed. The tip-sample force function is based on the Lennard-Jones potential with a nonlinearly parameterized unknown topography parameter. By estimating this parameter together with the tip-sample force using a nonlinear observer approach, the topography of the sample can be found. The observer and parameter estimator is shown to be exponentially stable. Simulation results are presented and compared to a more conventional extended Kalman filter.**

I. INTRODUCTION

Atomic force microscopy (AFM) [1] is a tool capable of studying and manipulating matter down to the atomic scale. This has made it one of the fundamental tools within the field of nanotechnology.

Dynamic modes of AFM [2] are often used for imaging the sample. In these modes the cantilever is oscillated using a dither piezo located at the base of the cantilever. Steady-state signals such as amplitude or frequency of the cantilever position can be detected and will change as the cantilever approaches the sample. The distance to the sample can be kept constant by adjusting a vertically oriented z-piezoscanner to keep the amplitude- or frequency-signal constant in a feedback loop. The z-scanner position can then be recorded as the sample is scanned in a raster pattern along the lateral directions to produce a topography map of the sample. The scanning motion is produced by a nanopositioning stage located beneath the cantilever. Due to lightly-damped vibration dynamics of such devices they are often controlled in a feedback loop. Such controllers can be simple as in damping and tracking control schemes [3], [4], [5], or by employing more complex model-matching techniques such as $\mathscr{H}_\infty$-control [6], [7]. The latter schemes can be challenging to implement due to their computational complexity. However, this can be treated by employing model reduction [8], [9].

Dynamic modes of AFM can be limited in terms of spatial resolution due to their dependency on steady-state signals. For improved resolution, the error signal in the feedback loop of the z-scanner can be imaged [10]. Some studies have used higher harmonics to exploit additional information in the available signal [11], [12]. Higher harmonics can provide improved spatial resolution by utilizing the time-varying interaction force. Other studies try to exploit the transient response for more information [13]. Such methods are often observer-based, and can be used for directly controlling the interaction force [14], or for active Q-control [15], [16]. In active Q-control the cantilever stiffness – or quality factor – is virtually controlled. This can be exploited to reduce the time it takes for the transient to vanish, and allows for higher resolution and increased scanning bandwidth.

In this paper a novel approach is used for topography imaging. Topography and interaction force signals are estimated directly by using a state- and parameter estimator based on the results of Grip et al. [17]. To achieve this, the linear cantilever dynamics is placed in a closed loop with a model of the tip-sample interaction force. This interaction force is described by the nonlinear Lennard-Jones potential, which depends on the position of the cantilever and the sample topography. Thus, the system can be described as a linear system augmented by a nonlinearly parameterized topography signal, which is applicable for the methodology in [17].

The presented method is designed for noncontact mode where the tip of the cantilever is located in the attractive region of the interaction force. This method does not rely on steady-state signals, thus the transient information is exploited. Additionally, the presented scheme also provides an estimate of the interaction force, which can allow for more direct feedback control such as in [14]. This force measurement can also be used for applications such as force spectroscopy [18]. Estimation of interaction forces by use of observers has been investigated in optical probing systems [19], but to the authors' best knowledge no previous observer-based techniques for topography estimation have included a model of the tip-sample interaction force.

The paper is organized as follows. In Section II the modeling of the system is presented. The state- and parameter estimation scheme is presented in Section III. The simulation setup is described in Section IV. In Section V the simulation results are presented. The overall imaging scheme is discussed in Section VI. Finally, conclusions are given in Section VII.

II. SYSTEM MODELING

A. Cantilever Dynamics

The cantilever deflection subjected to the nonlinear interaction forces can be described by a Luré feedback system [20]. This model has proven effective for describing several

*This work was partly supported by the Research Council of Norway through the Centres of Excellence funding scheme, project No. 223254 – AMOS.

The authors are with the Department of Engineering Cybernetics, Norwegian University of Science and Technology, Trondheim, Norway. {ragazzon, jan.tommy.gravdahl, kristin.y.pettersen, eielsen}@itk.ntnu.no

properties – including stability – of the cantilever loop [21]. The model can be seen in Figure 1, where F_{exc} controls the force applied to the cantilever for oscillation, F_{ts} is the tip-sample interaction force, and θ represents the topography of the sample.

The motion of the cantilever deflection can be described by a second-order harmonic oscillator [13] given by the transfer function

$$G(s) = \frac{\frac{1}{m}}{s^2 + 2\omega_0\zeta s + \omega_0^2} \tag{1}$$

where ω_0 is the resonance frequency, ζ is the damping ratio, and m is the effective mass of the cantilever.

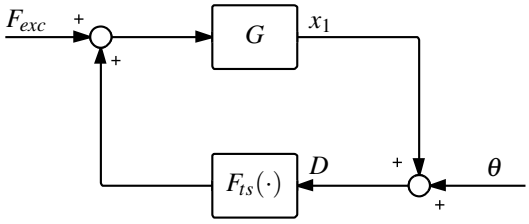

Fig. 1. Block diagram of the cantilever system. F_{exc} is controllable, while the cantilever deflection x_1 is the only measurable signal. The sample topography is represented by the signal θ.

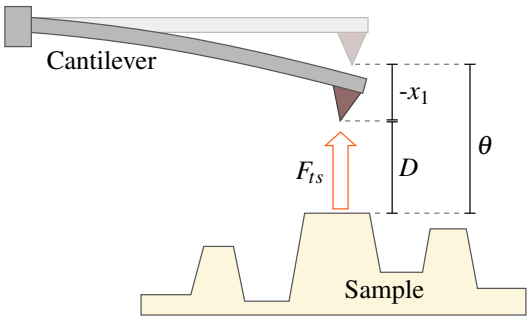

Fig. 2. Interaction between cantilever and sample, $D = x_1 + \theta$.

B. Tip-Sample Interaction Force

The interaction force between the probe tip and sample surface is nonlinear. Additionally, it has both an attractive region at large distances due to van der Waals-forces, and a repulsive region at very short distances due to electrostatic forces [22]. The attractive force can lead to an undesirable effect where the tip suddenly jumps into contact with the repulsive region of the force [23].

The interaction force between tip and sample can be described using the Lennard-Jones potential [24]

$$F_{ts}(D) = k_1 \left[\frac{\sigma^2}{D^2} - \frac{1}{30}\frac{\sigma^8}{D^8} \right] \tag{2}$$

where $D \triangleq x_1 + \theta$ is the tip-sample distance, x_1 is the cantilever deflection, θ is the unknown topography to be estimated, and $k_1 < 0, \sigma$ are parameters which depend on the physical and geometrical properties of the tip and the sample assumed to be known. The cantilever interaction with the sample is illustrated in Figure 2.

C. Noncontact Mode

As we operate the cantilever in noncontact mode, the following assumption introduces a monotonically increasing version of the Lennard-Jones potential, valid in this operating mode:

Assumption 1. *The modified force profile g is given by*

$$g(D) = \begin{cases} F_{ts}(D) & D > D_{cut} \\ S(D) & \text{otherwise} \end{cases} \tag{3}$$

$$S(D) = e^{r(D-D_{cut})}\left[F_{ts}(D_{cut}) - F_{ts}(D_0)\right] + F_{ts}(D_0) \tag{4}$$

where

$$\begin{aligned} D_0 &\triangleq \min_D F_{ts}(D) \\ &= \sigma\sqrt[6]{2/15} \end{aligned} \tag{5}$$

and $D_{cut} > D_0$ is a user-defined constant ideally set close to D_0.

To ensure sufficient smoothness of g, r needs to be solved from

$$\left.\frac{\partial S}{\partial D}\right|_{D_{cut}} = \left.\frac{\partial F_{ts}}{\partial D}\right|_{D_{cut}} \tag{6}$$

which gives

$$r = k_1 \frac{-2\sigma^2 D_{cut}^{-3} + \frac{8}{30}\sigma^8 D_{cut}^{-9}}{F_{ts}(D_{cut}) - F_{ts}(D_0)} \tag{7}$$

The interaction force F_{ts} is plotted with the modified force $g(D)$ in Figure 3 as a function of tip-sample distance for a given set of parameters.

Remark 1. The purpose of introducing a monotonically increasing modified force profile is to guarantee exponential stability of the nonlinear observer according to Theorem 1. Function $S(D)$ in (4) was chosen to provide a monotonically increasing force profile in the contact regime with a smooth transition to the traditional Lennard-Jones force curve $F_{ts}(D)$ in (2).

The operation in noncontact mode can be achieved either by feedback control of the z-piezo in the AFM or by controlling the cantilever oscillation amplitude. Alternatively, one can assume sufficiently small changes in the topography. Employing feedback control is outside the scope of this paper, but will be briefly presented in the simulations in Section IV–V. As such, we will make use of the following assumption:

Assumption 2. *The topography is assumed to be bounded, that is, there exist a known $\bar{\Theta} \in [\theta_{\min}, \theta_{\max}]$ such that $\theta \in \bar{\Theta}$.*

Additionally, the frequency of the driving signal for the cantilever oscillation should be set equal to or larger than the resonance frequency. When the tip approaches the surface, the attractive tip-sample force will effectively lower the resonance frequency of the cantilever. Thus, the amplitude will be reduced as the tip comes closer to the sample and is less inclined to approach the repulsive region [25].

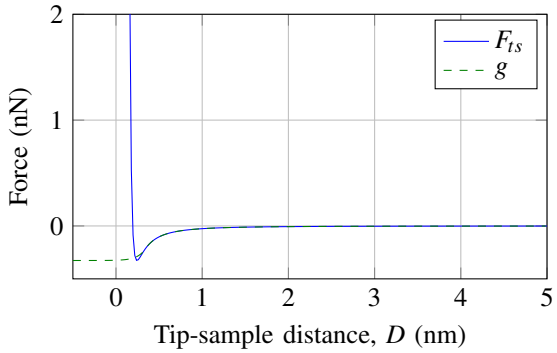

Fig. 3. The tip-sample interaction force resulting from the Lennard-Jones potential between a half-sphere and a flat surface, plotted with the modified force profile g employed by the nonlinear observer in noncontact mode.

III. STATE- AND PARAMETER ESTIMATOR

A. Overview

We utilize the methodology in [17] for estimation of states and parameters. The system depicted in Figure 1 can be written in an extended state-space form as

$$\begin{bmatrix} \dot{x} \\ \dot{\phi} \end{bmatrix} = \begin{bmatrix} A & E \\ 0 & 0 \end{bmatrix} \begin{bmatrix} x \\ \phi \end{bmatrix} + \begin{bmatrix} B \\ 0 \end{bmatrix} u + \begin{bmatrix} 0 \\ 1 \end{bmatrix} d \quad (8)$$

where the interaction force $g(x_1+\theta)$ has been introduced as a state ϕ and its time-derivative denoted as $\dot{\phi} \triangleq d(x,\theta)$, and the input u is the driving force of the cantilever.

The states $x \triangleq (x_1,x_2)^T$ of the system represent the cantilever deflection and the deflection velocity respectively, and the system matrices are given by

$$A = \begin{bmatrix} 0 & 1 \\ -\omega_0^2 & -2\zeta\omega_0 \end{bmatrix}, B = E = \begin{bmatrix} 0 \\ \frac{1}{m} \end{bmatrix}, C = \begin{bmatrix} 1 & 0 \end{bmatrix} \quad (9)$$

with $y = x_1$ as the only measurable signal. Let us also introduce the definition $\nu \triangleq \mathrm{col}(u,y)$ to simplify notation. The time-derivative of the interaction force can be found as

$$d(x,\theta) = \begin{cases} k_1\left[-2\sigma^2 D^{-3} + \frac{8}{30}\sigma^8 D^{-9}\right]x_2 & D > D_{cut} \\ re^{r(D-D_{cut})}\left[F_{ts}(D_{cut}) - F_{ts}(D_0)\right]x_2 & \text{otherwise} \end{cases} \quad (10)$$

where we have used $\dot{\theta} = 0$ which assumes that θ is slowly-varying compared to the rest of the dynamics. This will ultimately introduce a limitation to the lateral scanning speed that can be employed in order for the observer to properly track the topography. However, this will always be the case when imaging using any type of scanning probe microscope.

The modified high-gain observer of [17] is employed to estimate the states of this extended system, while the parameter estimator provides estimates for θ in (2) as depicted in Fig. 4. Estimates are denoted by a hat, e.g. $\hat{\theta}$.

The estimation scheme in [17] contains several assumptions that must be satisfied in order to guarantee stability.

Assumption 3. *The time derivative $\dot{u}$ is well defined and piecewise continuous; there exist compact sets $X \in \mathbb{R}^n, U \subset \mathbb{R}^m$, and $U' \subset \mathbb{R}^m$ such that for all $t \geq 0, x \in X, u \in U$, and $\dot{u} \in U'$.*

Assumption 4. *The triple (C,A,E) is left-invertible and minimum-phase.*

Assumption 5. *There exists a number $\beta > 0$ such that for all $(\nu,\dot{\nu},x,\theta,\phi) \in V \times V' \times X \times \Theta \times \Phi$ and for all $(\hat{x},\hat{\theta},\hat{\phi}) \in \mathbb{R}^n \times \Theta \times \mathbb{R}^k$, $\left\|d(\nu,\dot{\nu},x,\theta,\phi) - d(\nu,\dot{\nu},\hat{x},\hat{\theta},\hat{\phi})\right\| \leq \beta\left\|\mathrm{col}(x-\hat{x},\theta-\hat{\theta},\phi-\hat{\phi})\right\|$.*

These assumptions are satisfied as follows:

- A sinusoidal input signal u will be employed for oscillating the cantilever. The states x_1, x_2 are bounded due to the damped nature of the cantilever dynamics (1). Thus, Assumption 3 is satisfied.
- The system $G(s)$ has no invariant zeros, so it is left-invertible and minimum-phase and Assumption 4 is satisfied.
- Due to the smooth saturation introduced on g in (3), d becomes globally Lipschitz in terms of both x_1 and θ. Additionally, x_2 appears only linearly in (10) thus Assumption 5 is satisfied.

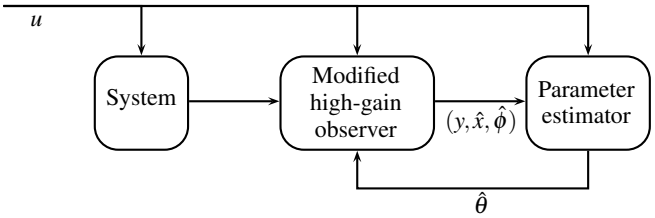

Fig. 4. Structure of the state- and parameter estimator. From [17].

B. Modified High-Gain Observer

By following the methodology in [17] a modified high-gain observer will be designed next where the estimated parameters are assumed to be available.

The observer is implemented as

$$\begin{aligned} \dot{\hat{x}} &= A\hat{x} + Bu + E\hat{\phi} + K_x(\varepsilon)(y - C\hat{x}) \\ \dot{z} &= -\frac{\partial g}{\partial \theta}\dot{\hat{\theta}} - \frac{\partial g}{\partial x}K_x(\varepsilon)(y - C\hat{x}) + K_\phi(\varepsilon)(y - C\hat{x}) \\ \hat{\phi} &= g(\hat{x}_1,\hat{\theta}) + z \end{aligned} \quad (11)$$

where the gains $K_x(\varepsilon), K_\phi(\varepsilon)$ are to be determined. By defining the errors $\tilde{x} \triangleq x - \hat{x}$, $\tilde{\phi} \triangleq \phi - \hat{\phi}$, we can find the error dynamics from (11). Our goal is to design the gains $K(\varepsilon) \triangleq \mathrm{col}(K_x(\varepsilon), K_\phi(\varepsilon))$ such that for a sufficiently small ε the error dynamics is input-to-state stable with respect to $\tilde{\theta} \triangleq \theta - \hat{\theta}$.

The error dynamics are found as

$$\begin{bmatrix} \dot{\tilde{x}} \\ \dot{\tilde{\phi}} \end{bmatrix} = \begin{bmatrix} 0 & 1 & 0 \\ 0 & 0 & 1 \\ 0 & -\omega_0^2 & -2\zeta\omega_0 \end{bmatrix} \begin{bmatrix} \tilde{x} \\ \tilde{\phi} \end{bmatrix} + \begin{bmatrix} 0 \\ 0 \\ 1 \end{bmatrix} \tilde{d} - \begin{bmatrix} K_x(\varepsilon) \\ K_\phi(\varepsilon) \end{bmatrix} \tilde{y} \quad (12)$$

The error dynamics are then transformed to the special coordinate basis (SCB). The Maple program developed in [26] was used for this purpose, resulting in the transformation matrices

$$\Lambda_1 = \begin{bmatrix} 1 & 0 & 0 \\ 0 & 1 & 0 \\ \omega_0^2 & 2\zeta\omega_0 & 1 \end{bmatrix}, \quad \Lambda_2 = [1], \quad \Lambda_3 = [m]$$

which transforms the system to the SCB in accordance with

$$\mathrm{col}(\tilde{x},\tilde{\phi}) = \Lambda_1\chi,\ \ \tilde{y} = \Lambda_2\gamma,\ \ \tilde{d} = \Lambda_3\delta$$

The observer gains can now be designed. Let $\bar{K}_q = \mathrm{col}(\bar{K}_{q_1},\ldots,\bar{K}_{q_3})$ be chosen such that the matrix

$$H \triangleq \begin{bmatrix} 1 & 0 & 0 \\ 0 & 1 & 0 \\ 0 & 0 & 0 \end{bmatrix} - \bar{K}_q \begin{bmatrix} 1 & 0 & 0 \end{bmatrix} \tag{13}$$

is Hurwitz using a pole-placement technique [17]. Then for our special case without any invariant zeros, the resulting gain is found from $K_q(\varepsilon) = \mathrm{col}(\bar{K}_{q1}/\varepsilon,\ldots,\bar{K}_{q3}/\varepsilon^3)$ and the transformation $K(\varepsilon) = \Lambda_1 K_q(\varepsilon)\Lambda_2^{-1}$. The poles of H were placed at $-1\pm 0.2i$ and -2, resulting in the gain

$$K(\varepsilon) = \begin{bmatrix} 4.0\varepsilon^{-1} \\ 5.04\varepsilon^{-2} \\ 4.0\omega_0^2\varepsilon^{-1} + 10.08\zeta\omega_0\varepsilon^{-2} + 2.08\varepsilon^{-3} \end{bmatrix} \tag{14}$$

The following Lemma from [17] ensures that this procedure for determining the gains will provide a stable estimate of the states with respect to $\tilde{\theta}$:

Lemma 1. *Assuming $\hat{\theta}\in\Theta$, there exists $0<\varepsilon^*\le 1$ such that for all $0<\varepsilon\le\varepsilon^*$, the error dynamics* (12) *is input-to-state stable with respect to $\tilde{\theta}$.*

C. Parameter Estimator

In the previous section a high-gain observer was designed based on known parameters. Next, we will design a parameter estimator for the topography signal which will be provided to the observer. An update law for the topography estimate $\hat{\theta}$,

$$\dot{\hat{\theta}} = u_\theta(\nu,\hat{x},\hat{\phi},\hat{\theta}) \tag{15}$$

must be found satisfying the following assumption from [17]:

Assumption 6. *There exist a differentiable function $V_u : \mathbb{R}_{\ge 0}\times(\Theta-\Theta)\to\mathbb{R}_{\ge 0}$ and positive constants $a_1,\ldots,a_4$ such that for all $(t,\tilde{\theta})\in\mathbb{R}_{\ge 0}\times(\Theta-\Theta)$,*

$$a_1\left\|\tilde{\theta}\right\|^2 \le V_u(t,\tilde{\theta}) \le a_2\left\|\tilde{\theta}\right\|^2$$
$$\frac{\partial V_u}{\partial t}(t,\tilde{\theta}) - \frac{\partial V_u}{\partial\tilde{\theta}}(t,\tilde{\theta})u_\theta(\nu,x,\phi,\theta-\tilde{\theta}) \le -a_3\left\|\tilde{\theta}\right\|$$
$$\left\|\frac{\partial V_u}{\partial\tilde{\theta}}(t,\tilde{\theta})\right\| \le a_4\left\|\tilde{\theta}\right\|$$

Furthermore, the update law (15) *ensures that if $\hat{\theta}(0)\in\Theta$, then for all $t\ge 0,\hat{\theta}\in\Theta$.*

Assumption 6 guarantees that the origin of the error dynamics

$$\dot{\tilde{\theta}} = -u_\theta(\nu,\hat{x},\hat{\phi},\theta-\tilde{\theta}) \tag{16}$$

where $\tilde{\theta}\triangleq\theta-\hat{\theta}$, is uniformly exponentially stable whenever $\hat{x}=x$ and $\hat{\phi}=\phi$.

In [27, Ch. 6], four propositions are stated in order to satisfy Assumption 6. Being a rational function with an 8th-degree polynomial in the denominator, it is difficult to solve $g(x_1+\theta)$ in terms of θ. Instead, a numerical search is performed to find the solution. We restate the following proposition from [27]:

Proposition 1 *Suppose that there exist a positive-definite matrix P and a function $M : V\times\mathbb{R}^n\times\Theta\to\mathbb{R}^{p\times k}$, such that for all $(\nu,x)\in V\times\mathbb{R}^n$ and for all pairs $\theta_1,\theta_2\in\Theta$,*

$$M(\nu,x,\theta_1)\frac{\partial g}{\partial\theta}(\nu,x,\theta_2) + \frac{\partial g}{\partial\theta}^T(\nu,x,\theta_2)M^T(\nu,x,\theta_1) \ge 2P \tag{17}$$

Then Assumption 6 is satisfied with the update law

$$u_\theta(\nu,\hat{x},\hat{\phi},\hat{\theta}) = \mathrm{Proj}\left(\Gamma M(\nu,\hat{x},\hat{\theta})(\hat{\phi}-g(\nu,\hat{x},\hat{\theta}))\right), \tag{18}$$

where Γ is a symmetric, positive-definite gain matrix.

Next, we need to choose an M such that (17) is satisfied. Let $M(\hat{D}) = M(\nu,\hat{x},\hat{\theta})$ where $\hat{D}\triangleq\hat{x}_1+\hat{\theta}$. We then choose

$$M(\hat{D}) = \tfrac{1}{2}M_{\max}\left[\tanh(M_{\mathrm{rate}}(\hat{D}-D_M))+1\right] \tag{19}$$

where $M_{\max}, M_{\mathrm{rate}}, D_M$ are tunable positive constants and $M(\hat{D})>0$ for any finite value of $\hat{D}$. Since our g and θ are scalar values, we have from (17),

$$2M(\nu,x,\theta_1)\frac{\partial g}{\partial\theta}(\nu,x,\theta_2) \ge 2P \tag{20}$$

To satisfy this inequality for some positive P, we want to show that $\partial g/\partial\theta$ is strictly positive in the domain of the arguments. We have

$$\frac{\partial g}{\partial\theta}(x,\theta) = \begin{cases} k_1\left[-2\sigma^2 D^{-3} + \frac{8}{30}\sigma^8 D^{-9}\right] & D > D_{cut} \\ re^{r(D-D_{cut})}\left[F_{ts}(D_{cut}) - F_{ts}(D_0)\right] & \text{otherwise} \end{cases} \tag{21}$$

The first case in (21) has only one real, positive root at the point $D=D_0$. Thus, $\frac{\partial g}{\partial\theta}$ never switches sign in $D>D_{cut}>D_0$. Above this point the negative D^{-3} term dominates, and since $k_1<0$, the result is positive. For the second case, we have that $F_{ts}(D_{cut})-F_{ts}(D_0)>0$, the exponential function is positive for all real, finite values, and r has the same sign as in the first case as evident from (7). Additionally, $\frac{\partial g}{\partial\theta}\neq 0$ for any finite value of D, assuming $k_1,\sigma\neq 0$.

Thus, the conditions of Proposition 6.3 are satisfied, and we can use the update law (18)–(19). The projection function in (18) ensures that the parameters $\hat{\theta}$ never leave Θ. For implementation details of this function we refer to [27].

Remark 2. Another feasible candidate for M is the choice $M=\frac{\partial g}{\partial\theta}$ as discussed in [27]. We found this choice to give wildly varying estimation speeds as the cantilever tip approached the sample. At the minimum tip-sample distance the update was very quick – limiting the update gain – while very slow anywhere else. The new choice of M in (19) gives a smoother transition of the estimation speed which allows us to increase the overall gain of the update law, providing better performance. Because the tip-sample force at large distances is very small, its detection will be dominated by noise. Thus, M is saturated by M_{max} in order to limit the update speed at large tip-sample distances.

D. Stability of Interconnected System

The interconnection between the modified high-gain observer (11) and the parameter estimator (15) also needs to be considered.

Assumption 7. *The parameter update law $u_\theta(\nu,\hat{x},\hat{\phi},\hat{\theta})$ is Lipschitz continuous in $(\hat{x},\hat{\phi})$, uniformly in $(\nu,\hat{\theta})$, on $V\times\mathbb{R}^n\times\mathbb{R}^k\times\Theta$.*

This assumption can be satisfied as follows:

- Consider the update law (18). We have that M in (19) is a saturated Lipschitz continuous function because of its dependency on the $\tanh(\cdot)$-function. We also have that $\partial g/\partial x_1 = \partial g/\partial\theta$ given in (21) is continuous and bounded. Thus g is Lipschitz continuous both in terms of x_1 and θ. The projection function in the update law does not change the Lipschitz properties as discussed in [27]. Thus, Assumption 7 is satisfied.

Finally, the following theorem based on [17, Th. 1] establishes the stability of the interconnected system:

Theorem 1. *If Assumption 1 – 7 are satisfied and $\hat{\theta}(0)\in\Theta$, there exists $0<\varepsilon^*\leq 1$ such that for all $0<\varepsilon\leq\varepsilon^*$, the origin of the error dynamics of the observer* (12) *and parameter estimator* (16) *is exponentially stable.*

Remark 3. Note that the system is globally exponentially stable with respect to the observer error states, i.e. it is only the parameter estimates that have limitations on their initial values.

E. Extended Kalman Filter

In order to provide a more detailed discussion on the performance of the nonlinear approach, an extended Kalman filter (EKF) was implemented for comparison. EKF is a well-established method for estimating the states of a nonlinear system, see e.g. [28].

The system as described in Section II can be modeled by the following set of equations:

$$\begin{aligned}\dot{x}_1 &= x_2\\ \dot{x}_2 &= -\omega_0^2 x_1 - 2\zeta\omega_0 x_2 + \tfrac{1}{m}u + \tfrac{1}{m}F_{ts}(D)\\ \dot{D} &= x_2 + w\\ y &= x_1 + v\end{aligned} \tag{22}$$

where the zero-mean white process noise w models the changes in topography with covariance Q, and v is zero-mean white measurement noise with covariance R.

The observer was implemented by using the continuous-time extended Kalman filter described in [28]. From the state estimates, the topography θ can be found from $\theta = D - x_1$ and the estimated interaction force is found by calculating $F_{ts}(D)$.

IV. SIMULATION SETUP

A simulation of the system has been set up with the system dynamics and estimation laws described in the previous sections. The parameters used in the simulation are given in Table I. A sinusoidal input signal is used for the cantilever giving it a freely oscillating amplitude of 100 nm. An oscillating cantilever is chosen in order to avoid the jump-to-contact behavior thereby satisfying Assumption 1. Initial distance to the sample is set to 105 nm from the resting position of the cantilever, while the topography is modeled as a square-like wave. The interaction force parameters σ, k_1 in (2) are based on values and formulas from [22].

The cantilever position is only controlled by a feedforward signal. Thus, over cavities in the sample the tip-sample distance will increase, and ultimately reduce the interaction force. This does affect the performance of the observers. To compensate for this, one simulation was run with a feedback controller to illustrate some possibilities for actual implementation. The feedback controller uses the estimated tip-sample distance $\hat{D} = \hat{x}_1 + \hat{\theta}$ to find the closest approach distance each cycle. A P-controller on the error between this signal and a reference distance is then used to control the amplitude of the cantilever oscillations.

Simulations were run both with and without additive white noise on the output of the cantilever deflection measurement, in order to discuss the effects of noise on the system. Note that the actual force F_{ts} in (2) is used in the plant dynamics to provide a more physically accurate simulation.

TABLE I
SIMULATION PARAMETERS

Param.	Value	Param.	Value
ω_0	1000 Hz	M_{max}	10^{-5}
ζ	0.005	M_{rate}	5×10^{4}
m	1.5728×10^{-9} kg	D_M	10^{-5}
σ	3.41×10^{-10} m	D_{cut}	D_0+10^{-10} m
k_1	-2.2242×10^{-10} N	Q	10^{-6}
ε	10^{-5}	R	10^{-16}
Γ	5×10^{4}	$u(t)$	$6.21\times10^{-11}\sin(\omega_0 t)$ [N]

V. RESULTS

The simulation results are plotted in Figure 5 – Figure 10.

Figure 5 shows the estimated topography parameter $\hat{\theta}$ plotted together with the actual topography. It can be seen that the estimates from both the nonlinear observer and the extended Kalman filter (EKF) are reasonably accurate. In Figure 6 it can be seen that the estimates have a staircase-like behavior. The steps occur when the cantilever position is at the bottom of its oscillation cycle, where the force interaction is the strongest. Far from the sample, the force field is so weak it does not provide any information on the distance.

After adding output noise to the simulations, we had to increase the ε-value and reduce the gain Γ of the nonlinear observer to give sufficiently accurate estimations. However, this resulted in some loss in performance as seen in Figure 7, noticeable by the slightly slower response and small drifting when the cantilever oscillates far from the surface over the sample cavities. The closest tip-sample distance each oscillation cycle is plotted in Figure 8, which varies with the topography due to the lack of feedback control.

With the feedback controller turned on the nonlinear observer regains some of its lost performance after adding output noise, as seen in Figure 9. Both observers also provide

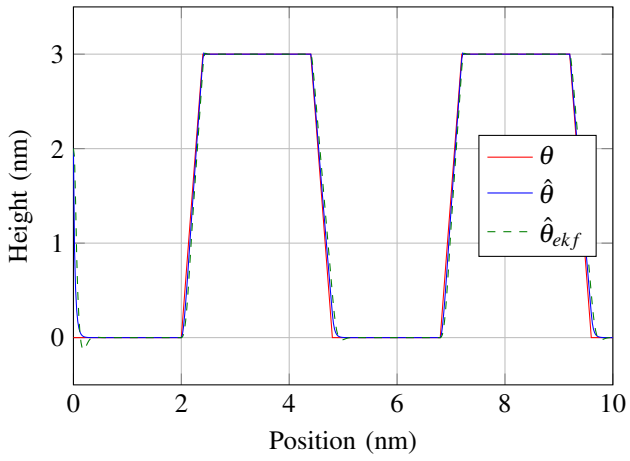

Fig. 5. Topography estimate.

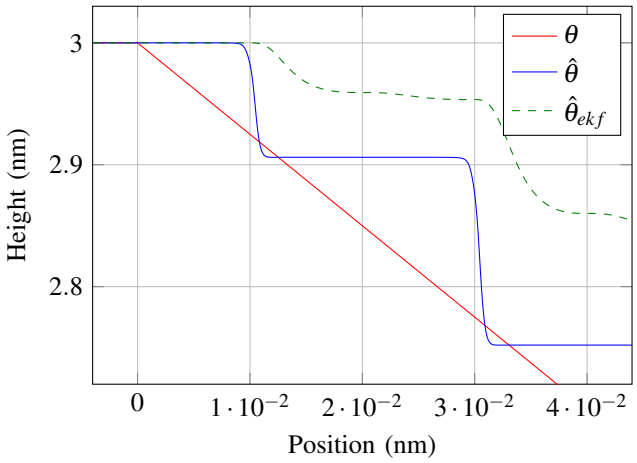

Fig. 6. Zoom of topography estimate. Position offset by 4.4 nm.

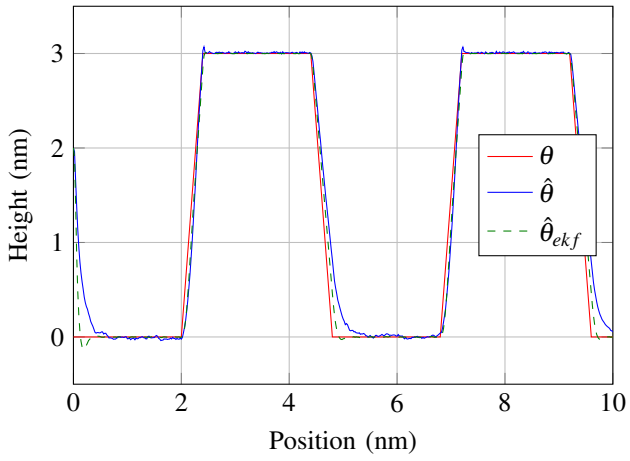

Fig. 7. Topography estimate with output noise. To attenuate the effects of noise ε was increased by a factor of 15 and Γ reduced by a factor of 4, which results in a slower response especially at large tip-sample distances.

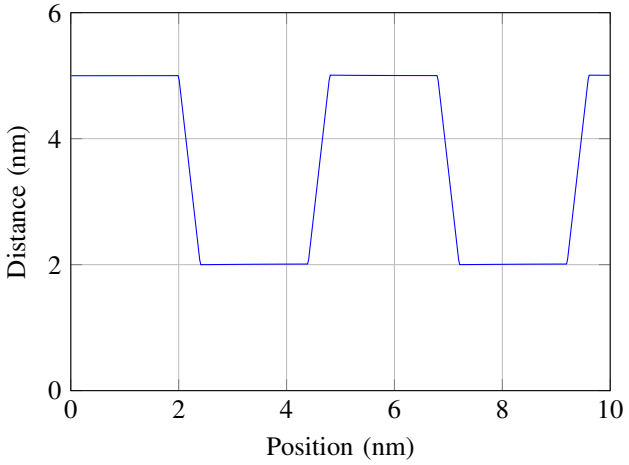

Fig. 8. Closest tip-sample distance D each oscillation cycle without feedback control.

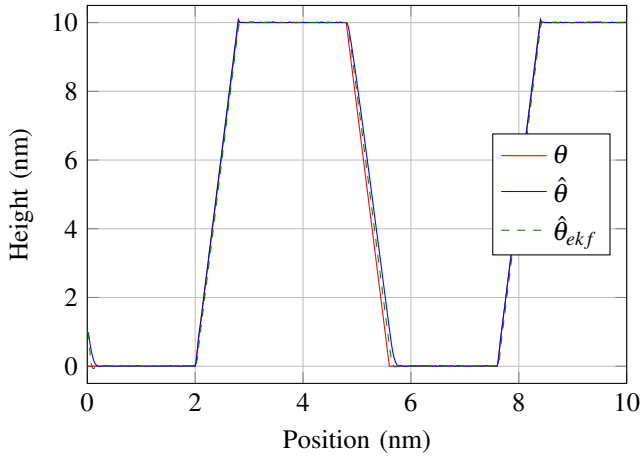

Fig. 9. With output noise and feedback control. This allows for scanning larger height differences and reduced gains which attenuates some of the noise.

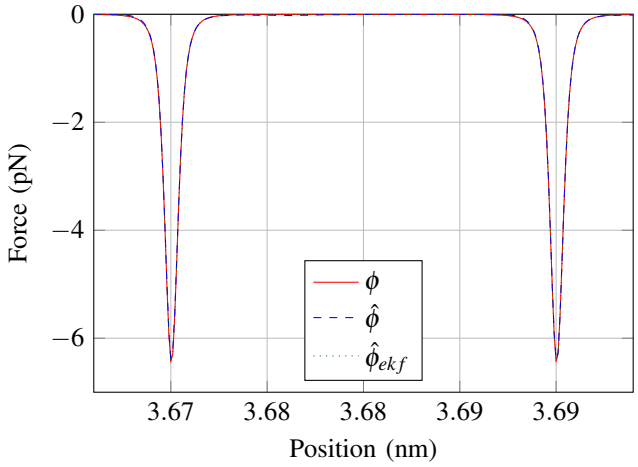

Fig. 10. Estimated interaction force ϕ with noise.

an estimate of the tip-sample interaction force as seen in Figure 10.

VI. DISCUSSION

The results demonstrate the efficiency of both the nonlinear observer (NLO) scheme and extended Kalman filter (EKF). The advantage of the NLO is its near-global exponential stability results as given in Theorem 1. The results suggest that the EKF provides a somewhat better trade-off between noise attenuation and response time. However, this could possibly be due to the tuning of the parameters.

The choice of M in (19) was based on an improvised approach after studying the observed characteristics of the NLO. Possibilities for further improvements to this function is considerable, as it is only required to be positive definite and to satisfy the Lipschitz conditions of Assumption 7.

For studying highly inhomogeneous samples the parameters in the Lennard-Jones potential in (2) would need to be estimated simultaneously. This can be achieved by including them in the parameter estimator of the nonlinear observer. This should be possible with relative ease, as a reformulation of these parameters will make them appear linearly in (2).

Ongoing work includes adopting the nonlinear observer scheme to tapping mode operation and experimental studies on an AFM.

VII. CONCLUSIONS

In this paper we have introduced a novel imaging technique for noncontact operation mode in AFM based on observers. Two distinct observer schemes were presented to show the viability of this technique, both of which directly estimates the tip-sample interaction force and topography of the sample. The nonlinear observer shows well-defined exponential stability results. A simulation study confirms the stability and convergence properties of the analysis. The second observer – based on an extended Kalman filter – show good performance in terms of accuracy and noise tolerance, but the nonlinear observer has stronger stability properties.

ACKNOWLEDGMENT

The authors would like to thank Håvard F. Grip for the useful and interesting correspondence.

REFERENCES

[1] G. Binnig, C. F. Quate, and C. Gerber, "Atomic Force Microscope," *Phys. Rev. Lett.*, vol. 56, no. 9, pp. 930–933, 1986.

[2] R. Garcia and R. Perez, "Dynamic atomic force microscopy methods," *Surface science reports*, vol. 47, pp. 197–301, 2002.

[3] A. A. Eielsen, M. Vagia, J. T. Gravdahl, and K. Y. Pettersen, "Damping and Tracking Control Schemes for Nanopositioning," *Mechatronics, IEEE/ASME Transactions on*, vol. 19, no. 2, pp. 432–444, 2013.

[4] S. S. Aphale, B. Bhikkaji, and S. O. R. Moheimani, "Minimizing scanning errors in piezoelectric stack-actuated nanopositioning platforms," *Nanotechnology, IEEE Transactions on*, vol. 7, no. 1, pp. 79–90, 2008.

[5] A. J. Fleming, "Nanopositioning system with force feedback for high-performance tracking and vibration control," *Mechatronics, IEEE/ASME Transactions on*, vol. 15, no. 3, pp. 433–447, 2010.

[6] G. Schitter, P. Menold, H. F. Knapp, F. Allgöwer, and A. Stemmer, "High performance feedback for fast scanning atomic force microscopes," *Review of Scientific Instruments*, vol. 72, no. 8, pp. 3320–3327, 2001.

[7] Y. K. Yong, K. Liu, and S. O. R. Moheimani, "Reducing cross-coupling in a compliant XY nanopositioner for fast and accurate raster scanning," *Control Systems Technology, IEEE Transactions on*, vol. 18, no. 5, pp. 1172–1179, 2010.

[8] M. R. P. Ragazzon, A. A. Eielsen, and J. T. Gravdahl, "H-inf Reduced Order Control for Nanopositioning: Numerical Implementability," in *19th IFAC World Congress, Proceedings of the*, Cape Town, South-Africa, 2014, pp. 6862–6869.

[9] J. Dong, S. M. Salapaka, and P. M. Ferreira, "Robust MIMO control of a parallel kinematics nano-positioner for high resolution high bandwidth tracking and repetitive tasks," in *Decision and Control, 2007. 46th IEEE Conference on*. IEEE, 2007, pp. 4495–4500.

[10] T. Ando, T. Uchihashi, and T. Fukuma, "High-speed atomic force microscopy for nano-visualization of dynamic biomolecular processes," *Progress in Surface Science*, vol. 83, no. 7-9, pp. 337–437, 2008.

[11] R. Hillenbrand, M. Stark, and R. Guckenberger, "Higher-harmonics generation in tapping-mode atomic-force microscopy: Insights into the tipsample interaction," *Applied Physics Letters*, vol. 76, no. 23, pp. 3478–3480, 2000.

[12] O. Sahin, C. F. Quate, O. Solgaard, and F. J. Giessibl, "Higher Harmonics and Time-Varying Forces in Dynamic Force Microscopy," in *Springer Handbook of Nanotechnology*, B. Bhushan, Ed. Springer Berlin Heidelberg, 2010, pp. 711–729.

[13] D. R. Sahoo, A. Sebastian, and M. V. Salapaka, "Transient-signal-based sample-detection in atomic force microscopy," *Applied Physics Letters*, vol. 83, no. 26, pp. 5521–5523, 2003.

[14] Y. Jeong, G. R. Jayanth, S. M. Jhiang, and C.-H. Menq, "Direct tip-sample interaction force control for the dynamic mode atomic force microscopy," *Applied Physics Letters*, vol. 88, no. 20, 2006.

[15] D. R. Sahoo, T. D. Murti, and V. Salapaka, "Observer based imaging methods for Atomic Force Microscopy," in *Proceedings of the 44th IEEE Conference on Decision and Control*, 2005, pp. 1185–1190.

[16] D. R. Sahoo, P. Agarwal, and M. V. Salapaka, "Transient Force Atomic Force Microscopy: A New Nano-Interrogation Method," in *2007 American Control Conference*, 2007, pp. 2135–2140.

[17] H. F. Grip, A. Saberi, and T. A. Johansen, "Estimation of states and parameters for linear systems with nonlinearly parameterized perturbations," *Systems & Control Letters*, vol. 60, no. 9, pp. 771–777, 2011.

[18] M. Morgenstern, A. Schwarz, and U. D. Schwarz, "Low-Temperature Scanning Probe Microscopy," in *Springer Handbook of Nanotechnology*, B. Bhushan, Ed. Springer Berlin Heidelberg, 2010, pp. 663–709.

[19] Y. Huang, P. Cheng, and C.-H. Menq, "Dynamic Force Sensing Using an Optically Trapped Probing System," *Mechatronics, IEEE/ASME Transactions on*, vol. 16, no. 6, pp. 1145–1154, 2011.

[20] A. Sebastian, M. V. Salapaka, D. J. Chen, and J. P. Cleveland, "Harmonic analysis based modeling of tapping-mode AFM," in *American Control Conference, 1999. Proceedings of the*, 1999, pp. 232–236.

[21] A. Sebastian, A. Gannepalli, and M. V. Salapaka, "A Review of the Systems Approach to the Analysis of Dynamic-Mode Atomic Force Microscopy," *IEEE Transactions on Control Systems Technology*, vol. 15, no. 5, pp. 952–959, 2007.

[22] D. Sarid, *Scanning force microscopy*. New York: Oxford University Press, 1994.

[23] F. J. Giessibl, "Advances in atomic force microscopy," *Reviews of modern physics*, vol. 75, no. 3, pp. 949–983, 2003.

[24] D. Y. Abramovitch, S. B. Andersson, L. Y. Pao, and G. Schitter, "A Tutorial on the Mechanisms, Dynamics, and Control of Atomic Force Microscopes," in *2007 American Control Conference*. IEEE, 2007, pp. 3488–3502.

[25] A. Schirmeisen, B. Anczykowski, H. Hölscher, and H. Fuchs, "Dynamic Modes of Atomic Force Microscopy," in *Springer Handbook of Nanotechnology*, B. Bhushan, Ed. Springer Berlin Heidelberg, 2010, pp. 731–761.

[26] H. F. Grip and A. Saberi, "Structural decomposition of linear multivariable systems using symbolic computations," *International Journal of Control*, vol. 83, no. 7, pp. 1414–1426, 2010.

[27] H. F. Grip, "Topics in State and Parameter Estimation for Nonlinear and Uncertain Systems," PhD Thesis, Norwegian University of Science and Technology, 2010.

[28] D. Simon, *Optimal State Estimation*. New York: Wiley, 2006.